Faraday Discussions

Linear ether-based highly concentrated electrolytes for Li-sulfur batteries

Journal:	*Faraday Discussions*
Manuscript ID	FD-ART-02-2024-000024.R1
Article Type:	Paper
Date Submitted by the Author:	19-Mar-2024

Complete List of Authors:	Ishikawa, Toru; Yokohama National University Haga, Shohei; Yokohama National University Shigenobu, Keisuke; Okayama University Sudoh, Taku; Yokohama National University Tsuzuki, Seiji; Yokohama National University, Institute of Advanced Sciences Shinoda, Wataru; Okayama University, Department of Chemistry Dokko, Kaoru; Yokohama National University, Department of Chemistry and Biotechnology Watanabe, Masayoshi; Yokohama National University, Chemistry andBiotechnology Ueno, Kazuhide; Yokohama National University, Department of Chemistry and Biotechnology

Linear ether-based highly concentrated electrolytes for Li-sulfur batteries

Toru Ishikawa [1], Shohei Haga [1], Keisuke Shigenobu [3], Taku Sudoh [1], Seiji Tsuzuki [2], Wataru Shinoda [3], Kaoru Dokko [1,2], Masayoshi Watanabe [2], Kazuhide Ueno [1,2]

1 Department of Chemistry and Life Science, Yokohama National University, 79-5 Tokiwadai, Hodogaya-ku, Yokohama, Kanagawa, 240-8501, Japan

2 Institute of Advanced Science, Yokohama National University, 79-5 Tokiwadai, Hodogaya-ku, Yokohama, Kanagawa, 240-8501, Japan

3 Research Institute for Interdisciplinary Science, Okayama University, 3-1-1 Tsushimanaka, Kita-ku, Okayama, Okayama, 700-8530, Japan

KEYWORDS: polysulfide solubility, donor property, Li ion coordination, ion transport, Li-S batteries

ABSTRACT

Li-S batteries have attracted attention as next-generation rechargeable batteries owing to their high theoretical capacity and cost-effectiveness. Sparingly solvating electrolytes hold promise because they suppress the dissolution and shuttling of polysulfide intermediates to increase the Coulombic efficiency and extend the cycle life. This study investigated the solubility of polysulfide (Li_2S_8) in a range of liquid electrolytes, including organic electrolytes, highly concentrated electrolytes, and ionic liquids. The Li_2S_8 solubility was well correlated with the donor number (DN_{NMR}), estimated via ^{23}Na-NMR, and was lower than 100 mM_(elemental sulfur) in electrolytes with DN_{NMR}<14, regardless of the type of electrolyte. Highly concentrated electrolytes comprising lithium bis(trifluoromethanesulfonyl)amide (LiTFSA) and linear chain dialkyl ethers such as methyl propyl ether (MPE), n-butyl methyl ether (BME), and ethyl propyl ether (EPE) were studied as sparingly solvating electrolytes for Li-S batteries. Monomethyl ethers, such as BME, showed more pronounced Li-ion coordination and higher ionic conductivity, whereas the steric hindrance of longer alkyl chains in EPE lowered the solvation number, enhanced ion association, and lowered the ionic conductivity despite the solvents having similar dielectric constants. The charge-discharge rate capabilities of Li-S cells with dialkyl ether-based electrolytes were more impressive than those of cells with a localized high-concentration electrolyte using sulfolane (SL) and hydrofluoroether (HFE), $[Li(SL)_2][TFSA]$-2HFE. The higher rate performance was attributed to the superior Li-ion transport properties of the

dialkyl ether-based electrolytes. A pouch-type cell using lightweight $[Li(BME)_3][TFSA]$ demonstrated an energy density exceeding 300 Wh kg^{-1} under lean electrolyte conditions.

Introduction

Lithium-sulfur (Li-S) rechargeable batteries (**Fig. 1a**) have recently attracted much attention because the theoretical capacity (1672 mAh g^{-1}) of the elemental sulfur (S_8) cathode is larger than that of the positive electrode materials used in conventional lithium-ion batteries.[1-3] However, many obstacles would need to be overcome before Li-S batteries would be ready for practical application. One critical problem is the dissolution of lithium polysulfides in electrolyte solutions (**Fig. 1b**). The solubilized polysulfides diffuse through the electrolyte and are chemically reduced at the Li metal anode, and the resulting reduced intermediate is electrochemically oxidized at the cathode during cell charging. This is known as the "redox shuttle" and this polysulfide shuttling has been the primary cause of failure of Li-S battery cycling.[4] In addition, carbonate solvents such as ethylene carbonate (EC) and diethyl carbonate (DEC), employed in commercial Li-ion batteries, cannot contend with the conditions in Li-S batteries because the polysulfide reacts irreversibly with these carbonates.[5] Currently, a mixed ether electrolyte such as dimethoxyethane (DME) and 1,3-dioxolane (DOL) containing about 1 M lithium bis(trifluoromethanesulfonyl)amide (LiTFSA) is mostly used as the electrolyte for Li-S batteries.[6] Although these electrolytes also readily dissolve polysulfide species, the redox shuttle can be prevented by an effective passivation layer formed through the parasitic decomposition of $LiNO_3$ additives and solvents on the Li metal anodes.[7]

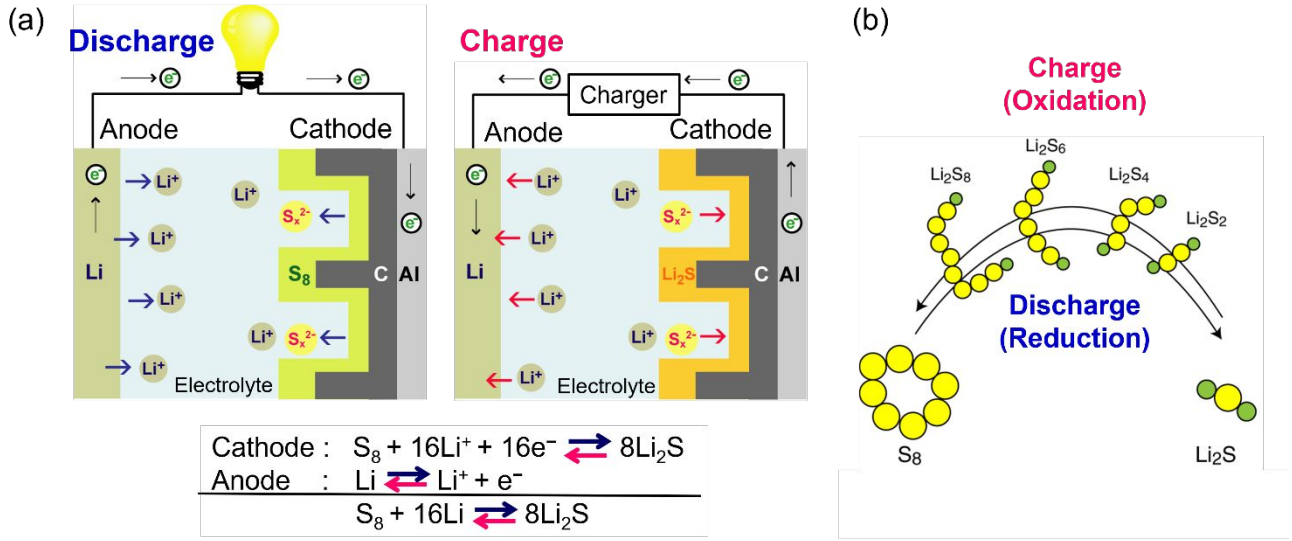

Fig. 1 Schematic diagrams of (a) Li-S batteries and charge–discharge reactions, and (b) lithium polysulfides formed in Li–S batteries during charge–discharge.

Sparingly solvating electrolytes have recently emerged as alternative liquid electrolyte materials for Li-S batteries.[8] The dissolution of polysulfide can be thermodynamically alleviated in this type of electrolyte, where the coordinating property towards lithium polysulfides is minimized by the judicious design of electrolyte solutions. The weakly coordinating properties of aprotic ionic liquids, such as TFSA-based ionic liquids, have been exploited to effectively suppress the dissolution of polysulfides.[9] Highly concentrated electrolytes (HCEs) with Li salt concentrations usually exceeding 3 M are prime examples of sparingly solvating electrolytes. Polysulfide dissolution can be effectively suppressed by a high salt concentration via the common ion effect[10] and the intrinsic scarcity of uncoordinated solvent molecules that have the potential to dissolve polysulfides in HCEs.[11, 12] Highly viscous HCEs have been further diluted with non-disrupting diluents such as hydrofluoroethers (HFEs)

with the intent of improving the fluidity and transport properties while retaining their favorable electrochemical properties. The use of this type of electrolyte, now termed localized high-concentration electrolytes (LHCEs), is becoming the prevailing approach for achieving highly reversible Li metal batteries[13-16] as well as in Li-S battery research using sparingly solvating electrolytes.[17-20]

A challenge with implications of a more practical nature for Li-S batteries is to increase the energy density in the actual cell configuration.[21-23] It was recently recognized that smaller amounts of electrolytes and a higher mass loading of S cathodes are essential for achieving high-energy-density Li-S batteries of which the performance exceeds that of state-of-the-art Li-ion batteries. However, the simultaneous achievement of these two requirements is not straightforward: Li-S batteries with smaller amounts of electrolyte and thicker S electrodes are prone to detrimental non-uniform electrode reactions at both the S cathode and Li metal anode, and eventually a rapidly decaying capacity. Therefore, much research effort has been devoted to the optimization of the electrode and electrolyte materials for successful charge-discharge cycling of high-energy-density Li-S batteries.[24-26] Specifically, liquid electrolytes require the following properties: (1) low solubility of sulfur and polysulfide species to mitigate the redox shuttle, (2) high Li-ion transport to enable fast S-cathode kinetics and suppress Li dendrite formation, (3) high reduction stability to avoid consumption of the Li metal and electrolyte, (4)

high chemical stability to withstand a nucleophilic attack by polysulfide species and (5) low weight density to achieve high energy density with a minimal amount of electrolyte.

To further optimize the sparingly solvating electrolytes for high-energy-density Li-S batteries, we thoroughly investigated the correlation between the solubility of sulfur and polysulfide species and solvent parameters in various liquid electrolytes, including organic electrolyte solutions, aprotic ionic liquids, and HCEs. We then focused on emerging dialkyl ether-based electrolytes and elucidated the dependence of their transport properties on the Li salt concentration, including the viscosity, ionic conductivity, and Li ion transference number of these electrolytes. Structure–property correlations were also studied at the solvent/Li salt molar ratio (x) of 3/1 using Raman spectroscopy, density functional theory (DFT) calculations, and molecular dynamics (MD) simulations because the maximum conductivity was obtained at this composition. The charge–discharge rate performance of Li-S cells using dialkyl ether-based electrolytes was compared to that of cells using a previously reported sparingly solvating electrolyte based on LHCEs. Finally, the high energy density of the Li-S cells was demonstrated in a pouch-cell configuration with different amounts of electrolyte.

Experimental

Preparation of electrolytes

Battery-grade LiTFSA (Kishida Chemical) was mixed with the organic solvents in an appropriate molar ratio. For the solubility tests, 1 M LiTFSA was dissolved in acetic anhydride (Ac_2O), acetonitrile (AN), butyl propionate (BP), n-butyl methyl ether (BME), tert-butyl methyl ether (t-BME), dipropyl ether (DPE), dimethoxy ethane (DME), 1,4-dioxolane (DOL), dimethyl sulfoxide (DMSO), hexamethylphosphoric triamide (HMPA), methane sulfonylfluoride (MSF), methyl propionate (MP), and tetrahydrofuran (THF). Aprotic ionic liquids, *N*-butyl-*N*-methylpyrrolidinium dicyanamide [P14][$N(CN)_2$], *N*-butyl-*N*-methylpyrrolidinium tetracyanoborate ([P14][$B(CN)_4$]), and 1,2-dimethyl-3-propyl-imidazolium imidazolium tris(trifluoromethanesulfonyl)methide ([C_3dmim][CTf_3]) were obtained from Iolitec. Sulfolane (SL, Kishida Chemical), 1,1,2,2-tetrafluoroethyl 2,2,3,3-tetrafluoropropyl ether (HFE, Daikin Industries), methyl propyl ether (MPE), ethyl propyl ether (EPE) and BME were used to prepare the electrolyte solutions for the transport property and battery tests. All organic solvents were obtained from Kanto Chemical, Tokyo Chemical Industry or Fujifilm Wako Pure Chemical Industries, unless otherwise noted. Undehydrated solvents were dried over molecular sieves as necessary.

Solubility of Li_2S_8 and S_8

The solubilities of long-chain polysulfides (nominally Li_2S_8) and S_8 were measured according to previous studies.[27] Saturated solutions of Li_2S_8 were prepared by stirring suspensions of S_8 and Li_2S in each electrolyte in a molar ratio of 7:8 at 60 °C for 100 h, and then stored for 1 d at room temperature to ensure the precipitation of excess S_8 and Li_2S. For the highly volatile solvents, the solutions were stirred at 30 °C. The supernatant solution was filtered and diluted with 1 mol dm^{-3} LiTFSA in tetraglyme (G4) solution. The dissolved Li_2S_8 in the solution was electrochemically oxidized to S_8 in a two-compartment electrochemical cell with carbon cloth as the working electrode, lithium foil as the counter electrode, and a lithium-conducting glass ceramic (LICGC, Ohara) as the separator. The maximum absorption of S_8 oxidized from the polysulfides was recorded using a UV-vis spectrophotometer (UV-2500PC, Shimadzu). The saturated solubility was determined from the absorbance, dilution factor, and a calibration curve of S_8 in 1 mol dm^{-3} LiTFSA in G4 solution. In this study, the solubility is represented as the total atomic S concentration (mM_S). The experimental errors of the solubility were less than 10%.

Polarity of electrolytes

The donor number of electrolytes was estimated by ^{23}Na NMR spectroscopy using a 5 mmϕ coaxial NMR tube (Shigemi, SP-405). NMR samples were prepared using 3 mol dm^{-3} NaCl D_2O solution as a reference in the inner tube and the sample electrolyte containing 0.3 M

$NaClO_4$ or NaFSA in the outer tube. The ^{23}Na chemical shift (δ_{Na}) of the peak derived from the reference was set to 0 ppm, and the δ_{Na} value of the sample electrolyte was recorded. From the chemical shift, the donor number (DN_{NMR}) of each electrolyte was estimated using the previously reported empirical relationship between Gutmann's donor number (DN) and δ_{Na}.[28]

Computational studies

DFT calculations were conducted using the Gaussian 16 program.[29] The geometries of the 1:4 complex cations consisting of Li ions and dialkyl ethers, $[Li(\text{dialkyl ethers})_4]^+$, were optimized at the B3LYP/6-311++G** level of theory.[30] MD simulations using polarizable force fields were performed using the polarizable version of the MPDyn simulation software.[31] The previously reported OPLS-AA-based force field parameters for LiTFSA were used to model the polarizable force fields,[32, 33] whereas new parameters for BME and EPE were developed based on *ab initio* molecular orbital calculations based on MP2/6-311++G** level of theory. Details of the force fields and simulation procedure are reported in Electronic Supplementary Information (ESI, **Tables S1-5 and Fig. S1**).

The radial distribution function and accumulative coordination number (ACN) of the O and N atoms around the Li ions were calculated to investigate the solution structure. The radial

distribution function $g_{ij}(r)$ of the *j*-th segment around the *i*-th segment is calculated as follows:

$$g_{ij}(r) = \frac{1}{4\pi r^2 \Delta r} \frac{V}{N_j} \langle \Delta n_{ij}(r) \rangle, \quad \#(1)$$

where $\langle \Delta n_{ij}(r) \rangle$ is the average number of *j*-th segments found at a distance of r from the *i*-th segment, and the grid size of Δr was set to 0.1 Å. The ACN, $N_{ij}(r)$, was calculated as

$$N_{ij}(r) = \int_0^r \langle \Delta n_{ij}(r) \rangle dr \quad \#(2)$$

Measurement of transport properties

The ionic conductivity (σ) was measured by the electrochemical impedance method using VMP3 (Biologic) in the frequency range of 500 kHz–1 Hz with a voltage amplitude of 10 mV. The cell constants of the conductivity cells (two platinum black electrode cells) were determined using an aqueous solution of KCl (0.01 mol dm^{-3}). The viscosity (η) and density (d) were determined using a Stabinger viscometer (SVM 300, Anton Paar). The Li-ion transference number ($t_{Li^+}^{abc}$) under anion-blocking conditions was estimated by potentiostatic polarization combined with electrochemical impedance spectroscopy using a Li|Li symmetric cell.[34-36] The experimental details were reported previously.[37] Here, a R2032-type coin cell was assembled with disc-shaped Li foil (Honjo metal, 16 mm in diameter) and a porous glass filter paper (Advantec, GA55, diameter = 17 mm) soaked with each electrolyte to the amount of 80

μL. The $t_{\mathrm{Li}^+}^{\mathrm{abc}}$ measurements were performed using a ModuLab XM ECS electrochemical test system (Solartron Analytical).

Raman spectroscopy

Raman spectra were recorded on a Raman spectrometer with a 785 nm laser (NRS-4100, JASCO) with the spectral resolution of 4.5 cm^{-1}. The instrument was calibrated using a polypropylene standard. The samples were sealed in a capillary tube and their temperature was controlled using a Peltier microscope stage (TS62, INSTEC) with a temperature controller (mk1000, INSTEC).

Preparation of sulfur/carbon composite electrode and battery test

A sulfur/carbon composite was prepared by melt diffusion using a mixture of elemental sulfur (S_8, 73 wt%), porous carbon Ketjen Black (KB, Lion Corporation, 24 wt%), and Black Titanium Oxide (TiB, Mitsubishi Material, 3 wt%).[38] S_8, KB, and TiB were mixed using an agitating mortar, transferred to a screw vial, and heated at 157 °C for 12 h to allow the uniform distribution of S_8 into the pores of KB. Aqueous slurries were prepared by mixing the S_8/KB/TiB composite with carboxymethyl cellulose (CMC2200, Daicel Fine Chem) and styrene butadiene rubber (SBR, JSR Corporation) at a S_8/KB/TiB (73/24/3 wt%): CMC2200:

SBR weight ratio of 96.5:1.5:2. The resulting slurry was coated onto carbon-coated aluminum foil as a current collector and dried in an oven at 35 °C for 2 h. The sulfur contents of the electrode were 72.3 wt%. Subsequently, the electrodes were cut into disc-shaped (for coin cells, diameter = 13.8 mm) or rectangular (for pouch cells, the area is 16.65 cm^2) specimens, and dried overnight in an oven under vacuum at 50 °C. The ratio of the electrolyte volume to the sulfur weight is denoted as E/S [μL-electrolyte / mg-sulfur]. Coin cells (R2032-type) were assembled using the prepared composite cathode, a polyolefin separator, a Li metal foil anode, and an electrolyte. Pouch cells with the above electrolyte and electrode materials were also assembled in a dry room according to the previously published work.[39] Pouch cells were fabricated using a layer-by-layer process to laminate the cathode (coating of either one or both sides of a carbon-coated Al current collector, 45×37 mm), polyolefin separator (50×43 mm), and Li metal anode (50×40 mm). Galvanostatic charge-discharge tests on the Li-S cells were carried out in the voltage range of 1.0–3.3 V at 30 °C. The energy density of pouch cells was calculated based on the actual mass of the S cathode, separator, electrolyte, and theoretical amount of lithium anode, excluding the weight of the Al laminate film and tabs.

Result and Discussion

Why dialkyl ether solvents?

The dissolution of polysulfide species in the electrolyte, a consequence of the coordination of the Li ions in ionic lithium polysulfides with Lewis basic ligands such as solvent molecules and anions in the electrolyte, is a critical issue that degrades the charge-discharge performance of Li-S batteries. In previous studies, weakly coordinating liquid electrolytes with low donor ability, including ILs, highly concentrated electrolytes (HCEs), and localized high-concentration electrolytes (LHCEs), were found to be effective suppressants of polysulfide dissolution.[40] Here we conducted an in-depth investigation of the relationship between the saturated solubility of highly soluble Li_2S_8 and the solvent polarity parameter, the donor ability (DN_{NMR}) estimated from the ^{23}Na-NMR chemical shift (δ_{Na}) in various liquid electrolytes. Note that Li_2S_8 cannot be isolated and is the nominal formula prepared by mixing S_8 and Li_2S (S_8 : Li_2S = 7 : 8).[41] Although other polysulfides with different chain lengths can be formed via disproportionation reactions in each electrolyte, we hereafter denote the lithium polysulfides using the above composition as Li_2S_8 by assuming a complete reaction between S_8 and Li_2S without the occurrence of disproportionation reactions for the sake of simplicity. Our previous study showed the polysulfides are the most soluble at the composition of Li_2S_8.[9, 42, 43]

In **Fig. 2a**, the reported Li_2S_8 solubilities in the HCEs of [Li(glyme)]X and aprotic ILs are plotted as a function of DN_{NMR}.[9, 42, 43] The solubility data for [C_3dmim][CTf_3], [P14][$B(CN)_4$], and [P14][$N(CN)_2$] were also added to the figure to verify the relationship over a wide range of DN_{NMR}. The solubility of Li_2S_8 was less than 10^2 mM_S in the [Li(glyme)]X and aprotic

ILs with DN_{NMR} values lower than 10, whereas it exceeded 10^3 mM_S in most electrolytes with higher DN_{NMR}. This verifies that the dissolution of Li_2S_8 was dominated by the coordination of Li ions of Li_2S_8 with strongly Lewis basic ligands solvent and anions. To examine whether this trend is valid for other liquid electrolytes or only for highly condensed electrolyte systems such as ILs and HCEs, the correlation between the solubility of Li_2S_8 and DN_{NMR} in organic electrolyte solutions containing 1M LiTFSA was studied in the same manner (**Fig. 2b**). The relationship in these solutions was similar, and a low solubility of less than 10^2 mM_S was achieved in the organic electrolyte solutions with a DN_{NMR} less than 14, even with a relatively low salt concentration of 1 M. Thus, the dissolution of polysulfides (Li_2S_8) can be effectively suppressed in electrolytes with a DN_{NMR} less than 14, regardless of the type of electrolyte material, although there were some exceptions: [Li(G3)][OTf] and [Li(G3)]NO_3.

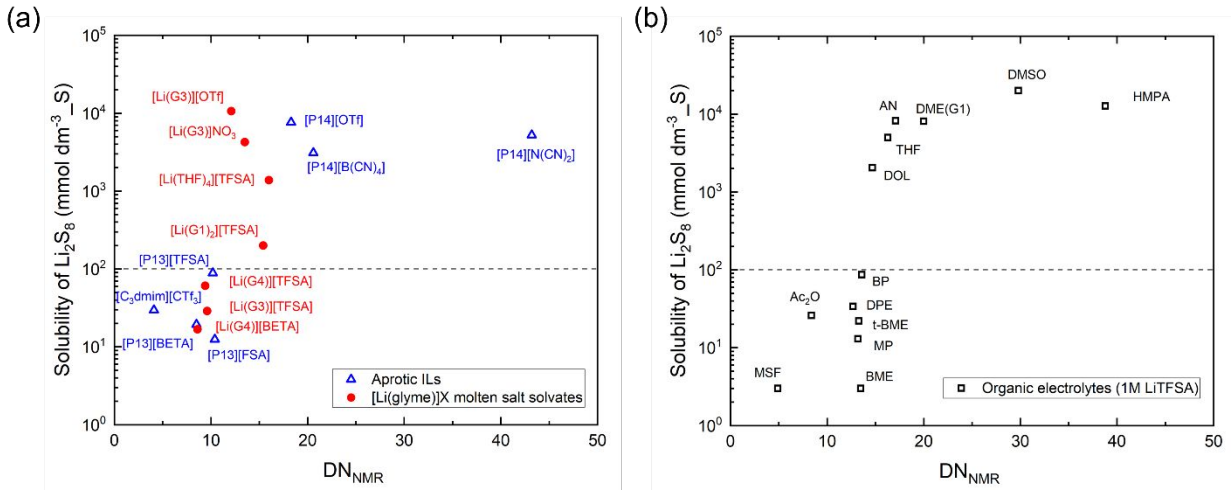

Fig. 2 Relationship between the solubility of polysulfide (Li_2S_8) and the donor number estimated from ^{23}Na-NMR (DN_{NMR}) in (a) aprotic ILs and [Li(glyme)]X molten solvates and (b) organic electrolyte solutions containing 1M LiTFSA. The horizontal dotted line represents the solubility limit of 10^2 mM_S. The solubility of polysulfide (Li_2S_8) in aprotic ILs and [Li(glyme)]X molten salt solvates was obtained from refs 42 and 43.

The dissolution of molecular sulfur, S_8, in the electrolytes also has the potential to cause the Li-S battery performance to deteriorate via the redox shuttling mechanism although dissolution of S_8 is much less significant than that of Li_2S_8. The compatibility of nonpolar materials such as nonionic polymers with solvents has often been discussed in association with the Hildebrand solubility parameter (δ).[44, 45] Two compounds can be predicted to be highly miscible if the δ values of the solute (δ_1) and solvent (δ_2) are similar, and the positive enthalpy change of mixing is minimized, $\Delta H_{\mathrm{mix}} \propto (\delta_1 - \delta_2)^2$, known as the "like dissolves like" principle. Based on this principle, the solubility of nonpolar S_8 was measured in selected molecular solvents and aprotic ILs and plotted as a function of their δ values (**Fig. 3**).[46-49] A higher solubility exceeding 10^2 mM_S was observed in the solvents with δ of ~ 10 (cal cm^{-3})$^{1/2}$, which is in good agreement with δ of the solute S_8, 10.2 (cal cm^{-3})$^{1/2}$, estimated from the literature values of the enthalpy of vaporization (ΔH_{vap}) and molar volume (V_{m}) using the equation, $\delta = \sqrt{(\Delta H_{\mathrm{vap}} - RT)/V_m}$, where R is the gas constant and T is the absolute temperature.[50] These results indicated that DN_{NMR} and δ are useful metrics for screening and designing sparingly solvating electrolytes capable of significantly suppressing the unfavorable dissolution of polysulfides and S_8.

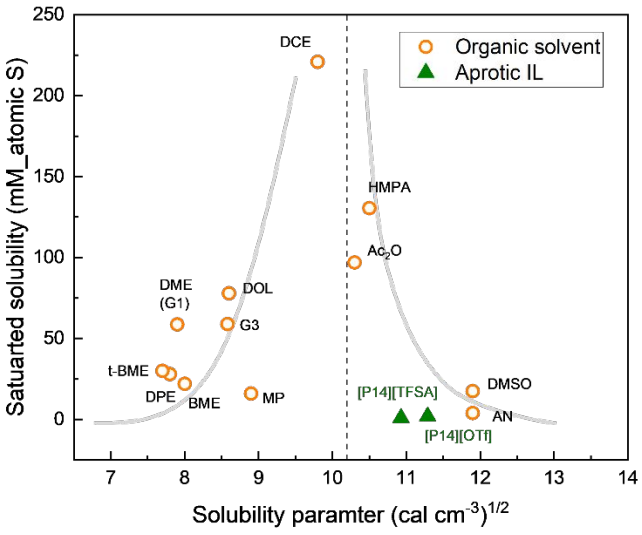

Fig. 3 Relationship between the solubility of molecular sulfur (S_8) and the Hildebrand solubility parameter (δ) in organic solvents and aprotic ILs. The vertical dotted line represents the estimated δ value (10.2 (cal cm^{-3})$^{1/2}$) of S_8. The gray curves are the guide for the eyes.

Li_2S_8 and S_8 are hardly soluble in dialkyl ethers (such as DPE, BME, and t-BME), esters (MP), MSF, and Ac_2O-based electrolytes, all of which are potential candidates for sparingly solvating liquid electrolytes. However, the electrolyte components used in Li-S batteries must satisfy other requirements, including multiple stabilities against Li metal electrodes and nucleophilic attack from polysulfide species. Our preliminary reactivity tests indicated that a small piece of Li metal foil irreversibly reacted with MP- and MSF-based electrolyte solutions, whereas Ac_2O was likely to undergo side reactions with polysulfide species, similar to carbonate solvents.[5] In contrast, the dialkyl ethers met all the key requirements and emerged as promising electrolytes for Li-S batteries. Indeed, a previous data-driven study revealed that dialkyl ether-based electrolytes demonstrated high

Coulombic efficiency (> 99.5%) of Li deposition/dissolution reactions for metallic Li anodes.[51] The dialkyl ether-based electrolytes were eventually selected for further testing as sparingly solvating electrolytes for Li-S batteries.

Ion transport properties and Li ion coordination in dialkyl ether-based electrolytes.

To optimize the formulation of dialkyl ether-based electrolytes, we first measured the ionic conductivity of a 1 M LiTFSA solution in the dialkyl ethers BME, t-BME, and DPE. The conductivity of t-BME and DPE-based electrolytes (0.18 and 0.17 mS cm^{-1} at 30 ˚C) was very low compared to that of the BME-based electrolyte (1.1 mS cm^{-1}) and were thereby eliminated from further investigations. Instead, we employed other linear ethers, EPE as structural isomers of BME, and MPE with shorter alkyl chain lengths. **Fig. 4** shows the dependence of the viscosity, ionic conductivity, Li-ion transference number measured under anion-blocking conditions ($t_{Li^+}^{abc}$), and density of the linear dialkyl ether-based electrolytes with LiTFSA on the salt concentration c_{Li}. The data of previously reported sparingly solvating electrolytes, sulfolane (SL)-based HCEs and LHCEs,[19, 20] $[Li(SL)_2][TFSA]$, and $[Li(SL)_2][TFSA]$-HFE, are shown in **Fig. 3** for comparison.

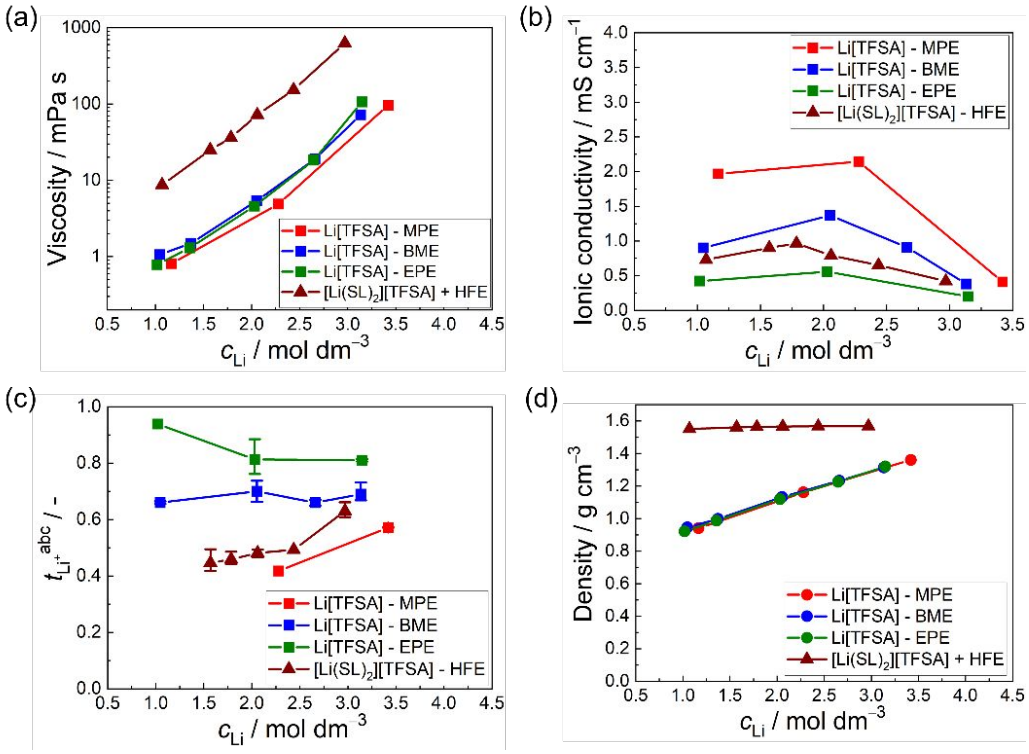

Fig. 4 Concentration dependence of (a) viscosity, (b) ionic conductivity, (c) Li ion transference number under anion-blocking conditions, and (d) density of the dialkyl ether-based electrolytes and SL-based HCE and LHCE diluted with HFE at 30 °C. Data for [Li(SL)$_2$][TFSA]-2HFE were obtained from ref. 20 except for $\boldsymbol{t}_{\mathbf{Li^+}}^{\mathbf{abc}}$.

The viscosity significantly increased by two orders of magnitude with the LiTFSA concentration increasing from 1.0 M in the organic electrolyte region to more than 3.0 M in the HCE region for all electrolytes studied (**Fig. 4a**). However, the viscosity of the dialkyl ether-based electrolyte was an order of magnitude lower than that of [Li(SL)$_2$][TFSA]-HFE at the same salt concentration, and the viscosity was the lowest for MPE-based electrolytes with shorter alkyl chain lengths. The highly viscous behavior of the SL-based electrolytes is attributable to the SL- and anion-bridged chain-like Li ion coordination structures, ···SL···Li$^+$···SL··· and ···TFSA$^-$···Li$^+$···TFSA$^-$···, wherein the two oxygen atoms of the SO_2 groups in SL and TFSA coordinate to two different Li ions.[20] The

viscosity of the dialkyl ether-based electrolytes are comparable to that of other ether-based electrolytes: e.g., the viscosity of DME(G1)-based electrolytes was reported to be 88 mPa s at c_{Li} of 3.4 M.[52] The difference in the chemical structure of the ether solvents is unlikely to significantly affect the viscosity of the ether-based electrolytes in the case of ether solvents with a fairly low molecular weight. As shown in **Fig. 4b**, the ionic conductivity reached a maximum value at ca. 2.0 M (i.e., [Li(dialkyl ether)$_3$][TFSA], corresponding to the solvent/LiTFSA molar ratio, x = 3/1) in the dialkyl ether-based electrolytes. The maximum conductivity of 2.2 mS cm^{-1} was achieved for the least viscous MPE-based electrolytes although the value is still markedly inferior to the conductivity of the carbonate-based electrolytes used in commercialized Li-ion batteries (~ 10 mS cm^{-1}). Despite their similar viscosities, the ionic conductivities of the BME- and EPE-based electrolytes were higher and lower than those of the reference data of the SL-based electrolytes, respectively. This is attributable to the difference in the degree of dissociation of LiTFSA in the BME- and EPE-based electrolytes. In addition, the change in the conductivity depending on the salt concentration is not as large as that reflected by the drastic viscosity change, suggesting that ion pairing or ion correlations that negatively affect ion conduction occur to some extent in the dialkyl ether-based electrolytes as well as in the SL-based LHCEs.

The Li ion transference number under anionic conditions ($t_{Li^+}^{abc}$) was estimated using potentiostatic polarization combined with electrochemical impedance spectroscopy in a Li|Li symmetric cell. In previous studies, SL-based HCEs and LHCEs were found to show relatively high $t_{Li^+}^{abc}$ values, which contributes to increasing the mass transfer of Li ions in Li-S cells and

eventually enhanced charge-discharge rate capability at higher current density.[39] Interestingly, compared to the SL-based HCE and LHCEs, the values of the transference number for MPE-based electrolytes are comparable ($t_{\mathrm{Li}^+}^{\mathrm{abc}}$ = 0.4~0.6) and are even higher ($t_{\mathrm{Li}^+}^{\mathrm{abc}}$ > 0.6) for the BME- and EPE-based electrolytes. For the dialkyl ether-based electrolytes, the values increase in the order of MPE < BME < EPE. Previous studies on $t_{\mathrm{Li}^+}^{\mathrm{abc}}$ based on the concentrated solution theory suggested that more ion-associative electrolyte systems can exhibit higher $t_{\mathrm{Li}^+}^{\mathrm{abc}}$ values as well as poor ionic conductivity: $t_{\mathrm{Li}^+}^{\mathrm{abc}}$ was found to be 0.93 in an ether-based HCE using highly associative lithium trifluoroacetate (LiTFA) where a high degree of clustering of Li and TFA ions was ascertained by high energy X-ray scattering experiments, molecular dynamics simulations, and the analysis of dynamic ion correlations.[37, 53] Likewise, the high $t_{\mathrm{Li}^+}^{\mathrm{abc}}$ values and relatively low ionic conductivity of the dialkyl ether-based electrolytes imply that ion pairing or ion association are pronounced even at the moderate c_{Li} of ~ 1.0 M and the extent thereof increases in the order of MPE < BME < EPE. In another report, the weakly coordinating properties of solvents that roughly correspond with the weak Lewis basicity of the anion were suggested to also afford high $t_{\mathrm{Li}^+}^{\mathrm{abc}}$ via frequent site-to-site exchange of Li ions in fluoroethylene carbonate-based HCEs using lithium bis(fluorosulfonyl)amide (LiFSA) salt with similar donor properties ($\mathrm{DN_{NMR}}$ = 7.9 and 8–10 for FEC and FSA, respectively).[54] The same might apply to dialkyl ether-based electrolytes owing to their low $\mathrm{DN_{NMR}}$ values (**Fig. 2b**).

Fig. 4d shows the dependence of the density on the concentration. As discussed later, the density of the electrolyte solution used in Li-S cells is a crucial factor for improving the energy density of Li-S batteries, where, under practical conditions, the cell is filled with a limited volume of electrolyte.[55-57] Lower electrolyte density values can improve the energy density by using a limited volume of electrolyte or by allowing a greater volume of electrolyte with the same energy density in the cell.

The previously reported SL-based HCEs and LHCEs largely consist of fluorinated components (TFSA and HFE) and thereby have density values higher than 1.5 g cm^{-3}. By contrast, the dialkyl ether-based electrolytes are lightweight with lower density values ranging from 0.9 to 1.3 g cm^{-3} depending on the salt concentration. In addition to the low solubility of the sulfur species and the stability towards Li metal and polysulfide nucleophiles, the low density is also a beneficial property of dialkyl ether-based electrolytes for Li-S batteries.

The Li-ion coordination structure was elucidated to understand the molecular origin of the observed differences in the transport properties of the dialkyl ether-based electrolytes. Because the coordination number of Li ions is known to be 4–5 in nonaqueous electrolyte solutions,[58, 59] we first performed DFT calculations for the corresponding 1:4 complex cations of Li ions and ether solvents. **Fig. 5** shows the optimized geometries of the $[Li(\text{dialkyl ether})_4]^+$ complexes. For $[Li(MPE)_4]^+$ and $[Li(BME)_4]^+$, the oxygen atoms of four ethers have close contact with Li ion in the optimized geometries with Li–O

coordination bond lengths of 2.04 Å. In sharp contrast, for $[Li(EPE)_4]^+$, oxygen atoms of three ethers have close contact (1.97 Å) with Li ion in the optimized geometry, whereas the remaining EPE is positioned far away from the Li ion with Li–O distance of 6.03 Å. The geometry optimizations of $[Li(t\text{-}BME)_4]^+$ and $[Li(DPE)_4]^+$ also confirmed that the 3-coordinated structures of Li complexes are stable (**Fig. S2**). Obviously, the monomethyl-terminated linear alkyl ethers (such as MPE and BME) enabled efficient packing of the solvent molecules around the Li ion, whereas the steric crowding of the longer or branched alkyl chains in EPE, t-BME, and DPE hindered the formation of the 4-coordinated Li complexes, which might in turn lead to more pronounced ion association.

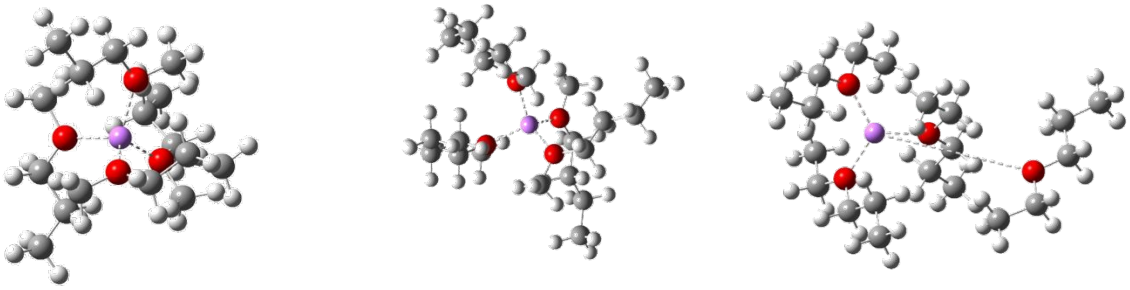

Fig. 5 Optimized geometries for $[Li(MPE)_4]^+$, $[Li(BME)_4]^+$ and $[Li(EPE)_4]^+$ complex cations optimized at the B3LYP/6-311G** level of theory. Purple: Li+, red: O, grey: C, and light grey: H.

The ion association of LiTFSA in actual electrolyte solutions was studied using Raman spectroscopy. **Fig. 6** shows the Raman spectra from 730 to 770 cm^{-1} for structurally isomeric BME- and EPE-based electrolytes with different solvent/LiTFSA molar ratios (x). The bands in this range

correspond to the CF_3 bending vibration coupled with the S-N stretching vibration of the TFSA anions and are sensitive to interactions with Li ions. The band at 739–742 cm^{-1} is assigned to spectroscopically free TFSA anions or solvent-separated ion pairs (SSIPs), and the band at 745–755 cm^{-1} is derived from a contact ion pair (CIP) or an aggregate (AGG) where the TFSA anion is bound directly to Li ions.[60-62] In both BME- and EPE-based electrolytes, the band at 749 cm^{-1} for $x = 7$ (c_{Li} ~ 1 M) underwent blueshift to a slightly larger wavenumber of 751 cm^{-1} for $x = 1.5$ (c_{Li} ~ 3 M) with peak broadening, suggesting a slight increase in the population of the higher ion aggregates. For the reference SL-based HCE and LCHEs, this peak of the TFSA anions emerged at a lower wavenumber (746 cm^{-1}) and underwent negligible shift with the addition of nonpolar HFE to the SL-based HCE.[20] Therefore, the ion association is considered more remarkable in the dialkyl ether-based electrolytes than the SL-based HCE and LHCEs. This could be primarily ascribed to the much lower dielectric constant (ε) of the dialkyl ethers (2.3 for both BME and EPE)[63] compared to SL ($\varepsilon = 44$)[64]: the strong cation-anion interaction in the low polarity solvents results in enhanced ion association. Although the Raman spectra of the BME- and EPE-based electrolytes did not appear to differ, these data suggest that LiTFSA exists mainly in the form of CIP and AGG in the linear dialkyl ether-based electrolytes, even at a moderate c_{Li} of ~1 M and in the HCE region.

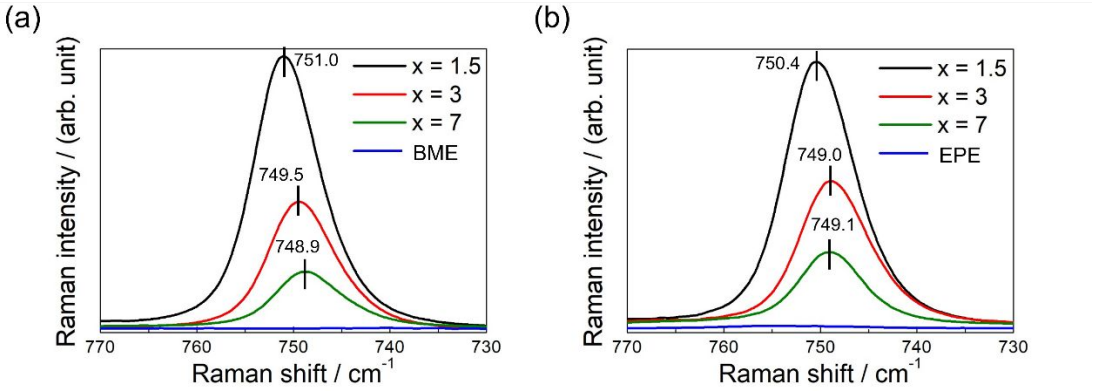

Fig. 6 Raman spectra of (a) BME- and (b) EPE-based electrolytes at different solvent/LiTFSA molar ratios (x) in the range of 730-770 cm^{-1} for TFSA at 30 °C.

We also performed MD simulations using a polarizable force field to investigate the solution structure in dialkyl ether-based electrolytes with a solvent/LiTFSA molar ratio (x) of 3/1. This composition is considered to be in the high-concentration region because of the lack of solvent sites to satisfy the number of solvated Li ions. **Fig. 7a and b** shows snapshots of the MD simulations of the structurally isomeric BME- and EPE-based HCEs, respectively. A notable feature of the obtained solution structure is spatial heterogeneity as is often observed in ionic liquids,[65, 66] HCEs,[67] and LCHEs.[68] The first coordination shell of the Li ions is defined as coordination by ether or TFSA oxygen atoms within 3 Å and is displayed as the red region in the simulation box. In both solutions, the coordination shells were interconnected to form polar domains that served as ion conduction paths. The alkyl chains of the ether solvents and the CF_3 groups of TFSA were excluded from the polar domains and aggregated into nonpolar domains. The differences in the nanosegregated solution

structure were not discernible in the snapshots of the BME- and EPE-based electrolytes. The differences in the solvation structure and ion association in these electrolytes were further elucidated using MD simulations.

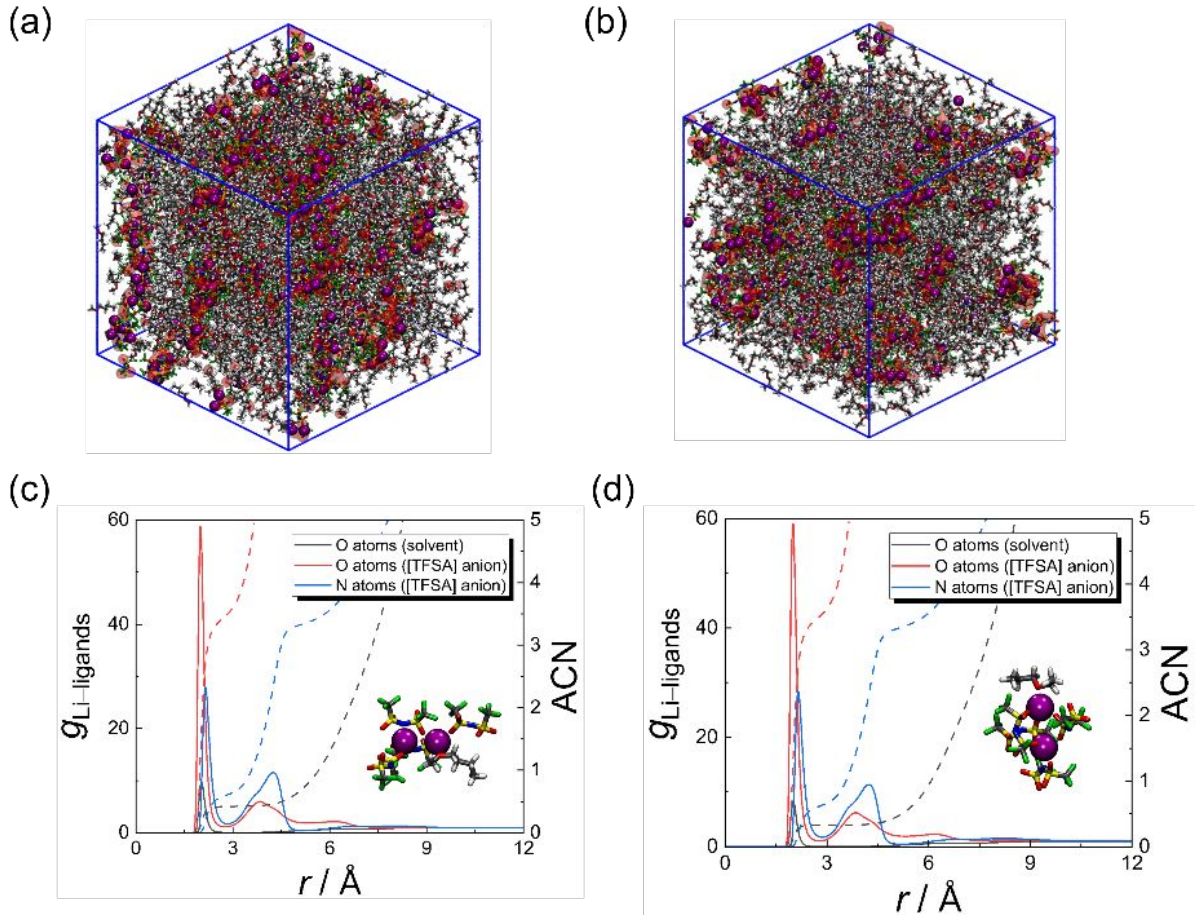

Fig. 7 Snapshots of the MD simulations of (a) BME- and (b) EPE-based HCEs at the solvent/LiTFSA molar ratio (*x*) of 3/1. The red volumes represent the surface of oxygen atoms in the first coordination shell of Li ions (Li[TFSA]/BME = 400/1200 and Li[TFSA]/EPE = 400/1200). Radial distribution functions around Li ions and accumulative coordination numbers of Li-O(solvent), Li-O(TFSA), Li-

N (TFSA) for (c) BME-based and (d) EPE-based HCEs at the solvent/LiTFSA molar ratio (x) of 3/1. The inset shows a representative coordination structure of the MD simulation.

Fig. 7c and d show the radial distribution functions between the Li ions and the possible coordinating sites, $g_{\text{Li-ligands}}$, O atoms of the ether solvents, and O and N atoms of TFSA, respectively. The accumulative coordination number (ACN) for each pair in the range of 0–12 Å is also shown. A sharp peak at 2.00 Å for the Li–O (solvent) pair in both dialkyl ether-based HCEs is attributed to the contact between Li ions and O atoms of the ether solvents, and is consistent with the Li–O coordination bond lengths in the optimized geometries of the complex cations as illustrated in **Fig. 5**. Well-resolved peaks for the Li–O (TFSA anion) and Li–N (TFSA anion) pairs were also observed at 2.00 Å and 2.15 Å, respectively, and were assigned to the coordination of TFSA with Li ions. The much higher intensity of the peak for the Li–O (TFSA anion) pair than that for the Li–O (solvent) pair clearly indicates that Li ion coordination is dominated by the TFSA anions rather than by solvent molecules, as depicted by the representative coordination structures in the insets of **Fig. 7c and d**. This observation qualitatively agrees with the Raman spectra, which show enhanced ion aggregation (**Fig. 6**). These structural aspects were not significantly different between the BME- and EPE-based HCEs. However, MD simulations indicated that the coordination number was slightly solvent dependent: the coordination numbers of O atoms of the solvent and O and N atoms of the anion

at 3.0 Å were 0.42, 3.60, and 0.64 in BME-based HCE, and 0.33, 3.63, and 0.66 in EPE-based HCE, respectively. This suggested that more ether molecules participated in Li-ion solvation for the BME-based HCE, although the majority of the solvent molecules remained uncoordinated in both dialkyl ether-based HCEs. As predicted by DFT calculations of the $[Li(\text{dialkyl ether})_4]^+$ complex cations (**Fig. 5**), the less sterically hindered coordination ability of the methyl-terminated, linear BME is responsible for a higher solvent coordination number. Alternatively, the coordination number of TFSA was slightly lower for the BME-based HCE, suggesting a lower degree of ion association.

Based on the classic theory of the ionic conduction mechanism, a lower degree of ion association can be the cause of the higher ionic conductivity and lower $t_{Li^+}^{abc}$ of the BME-based electrolytes, as shown in **Fig. 4b and c**. In addition, the ion aggregates of the weakly coordinating TFSA anions were transient, enabling rapid Li-ion exchange between the coordinating sites of the solvent and the anion. The weak coordinating property of dialkyl ether solvents is considered to play a role in ion conduction. Solvent molecules can serve as a temporary coordinating site for a Li ion to diffuse from one site to another, known as "solvent-assisted" Li-ion conduction in organic electrolytes,[69, 70] and metal−organic framework based quasi-solid-state electrolytes.[71] Such a conduction mechanism can also occur on the labile AGG networks found in the present systems (**Fig. 6a and b**) and would be more frequent in BME-based HCE with higher solvent coordination numbers, resulting in higher ionic conductivity.

Li-S battery performance.

We employed dialkyl ether-based electrolytes at an ether/LiTFSA molar ratio (x) of 3/1 ([Li(dialkyl ether)$_3$][TFSA]) in the Li-S battery tests because the maximum conductivity was observed at this composition in each electrolyte. **Table 1** summarizes the salt concentration, density, and transport properties of [Li(dialkyl ether)$_3$][TFSA] and the previously optimized SL-based LHCE, [Li(SL)$_2$][TFSA]-2HFE, at 30 °C. As discussed in the previous section, [Li(dialkyl ether)$_3$][TFSA] is generally lighter and less viscous than [Li(SL)$_2$][TFSA]-2HFE, despite its higher c_{Li} values. [Li(MPE)$_3$][TFSA] and [Li(BME)$_3$][TFSA] outperform [Li(SL)$_2$][TFSA]-2HFE in terms of ionic conductivity, whereas [Li(BME)$_3$][TFSA] and [Li(EPE)$_3$][TFSA] both have higher $t_{\mathrm{Li}^+}^{\mathrm{abc}}$ than [Li(SL)$_2$][TFSA]-2HFE. The Li_2S_8 solubility was determined to 10, 13, and 7 mM_S for [Li(MPE)$_3$][TFSA], [Li(BME)$_3$][TFSA], and [Li(EPE)$_3$][TFSA], respectively. These values are comparable to those of [Li(SL)$_2$][TFSA]-2HFE (5 mM_S)[20] and thereby [Li(dialkyl ether)$_3$][TFSA] is a sparingly solvating electrolyte for Li-S batteries (cf. Li_2S_8 solubility ~ 6600 mM_S for commonly used organic electrolytes, 1 M LiTFSA in DME/DOL).[19]

Table 1 Various properties of the electrolytes: salt concentration (c_{Li}), density (d), and viscosity (η), ionic conductivity (σ), and Li ion transference number under anion blocking condition ($t_{\mathrm{Li}^+}^{\mathrm{abc}}$) of [Li(dialkyl ether)$_3$][TFSA] and [Li(SL)$_2$][TFSA]-2HFE at 30 °C. Data for [Li(SL)$_2$][TFSA]-2HFE were obtained from ref. 20 except for $t_{\mathrm{Li}^+}^{\mathrm{abc}}$.

Electrolytes	c_{Li} / mol dm^{-3}	d / g cm^{-3}	η / mPa s	σ / mS cm^{-1}	$t_{Li^+}^{abc}$ / -	$\sigma \times t_{Li^+}^{abc}$ mS cm^{-1}
[Li(MPE)$_3$][TFSA]	2.28	1.16	4.9	2.2	0.42	0.90
[Li(BME)$_3$][TFSA]	2.05	1.13	5.4	1.4	0.70	0.96
[Li(EPE)$_3$][TFSA]	2.03	1.12	4.6	0.56	0.81	0.45
[Li(SL)$_2$][TFSA]-2HFE	1.57	1.56	25.0	0.90	0.45	0.40

Figure 8 shows the charge and discharge curves of the Li-S coin-type cells at different discharge C rates (current densities) and the same charge rate of 1/20 C. The discharge curves had two distinct voltage plateaus in all the Li-S cells. These plateaus correspond to the reduction of S_8 to higher-order polysulfides and the subsequent reduction of the polysulfides to shorter Li_2S_2 and Li_2S for the upper and lower voltage plateaus, respectively.[72] With increasing C-rate, these plateaus shift to a lower voltage level owing to an increase in the overpotential, leading to a loss of capacity.

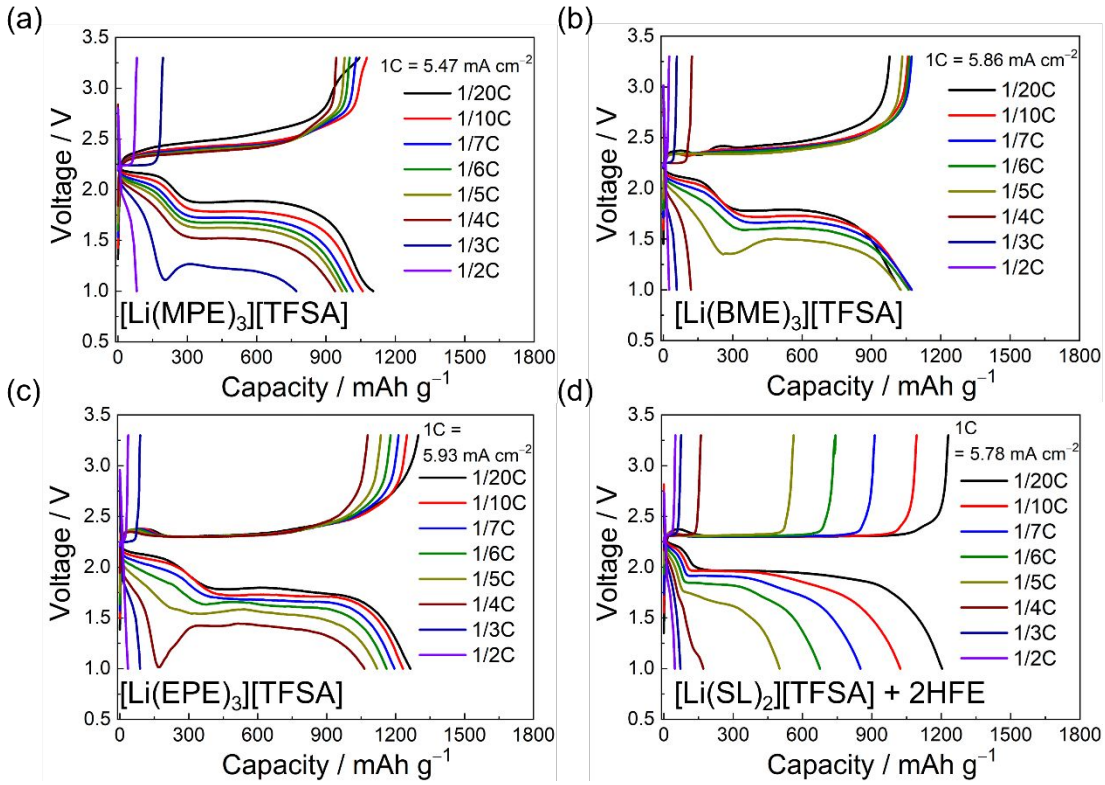

Fig. 8 Charge-discharge curves of Li-S coin-type cells using (a) [Li(MPE)$_3$][TFSA], (b) [Li(BME)$_3$][TFSA], (c) [Li(EPE)$_3$][TFSA], and (d) [Li(SL)$_2$][TFSA]-2HFE at various discharge current densities (1C = 5.5−6.0 mA cm^{-2}) with the cutoff voltage of 1.0 and 3.3 V at 30 ˚C. Sulfur loading: 3.4–3.6 mg cm^{-2}, E/S: 22−23 μL mg^{-1}, Current density: charge at 1/20 C, discharge from 1/20 C to 1/2 C.

The discharge curves, particularly at higher current densities, show two prominent differences between [Li(dialkyl ether)$_3$][TFSA] and [Li(SL)$_2$][TFSA]-2HFE. One is a voltage "dip," which can be observed at about 200−300 mAh g^{-1} for [Li(dialkyl ether)$_3$][TFSA], but not for [Li(SL)$_2$][TFSA]-2HFE. This voltage dip is attributed to the overpotential required for the

nucleation and initial growth of Li_2S on the sulfur cathode.[73] The larger overpotential in the voltage dip region suggests that the supply of polysulfides to the electrode is more restricted and the nucleation and growth of Li_2S becomes more sluggish in [Li(dialkyl ether)$_3$][TFSA]. This seems counterintuitive, because the solubilities of Li_2S_8 in these electrolytes are comparable. However, in actual Li–S cells, a salt concentration gradient forms across the cell during discharging, and the concentration of the solvent increases in the vicinity of the cathode surface. As shown in **Fig. 2b**, dialkyl ethers barely dissolved Li_2S_8 even with moderate c_{Li} values. On the other hand, higher order polysulfides may be more soluble in polar SL-based solution with a relatively high Guttmann donor number of 14.8 kcal mol^{-1}.[20] Accordingly, the low solubility of polysulfides in the dialkyl ether-based electrolytes limits the access of polysulfides to the electrode, resulting in the significant voltage dip (i.e., slow kinetics of the Li_2S nucleation and growth) during discharge at higher current densities. Another feature of the differences in the discharge curves is observed in the second plateau. In the discharge curves of the cell with [Li(SL)$_2$][TFSA]-2HFE (**Fig. 8d**), the cell voltage decreased steeply in the middle of the capacity range, and the second plateau accounted for a smaller capacity with increasing C-rate. In contrast, for the cells with [Li(dialkyl ether)$_3$][TFSA] (**Fig. 8a-c**), the second plateau following the voltage dip remained extended even at higher current densities. The higher capacity in the second plateau at higher C-rates was probably due to the superior mass transfer of Li ions in [Li(dialkyl ether)$_3$][TFSA]. Indeed, the Li ion transport property,

estimated by $\sigma \times t_{Li^+}^{abc}$, was higher for [Li(dialkyl ether)$_3$][TFSA] compared to that of [Li(SL)$_2$][TFSA]-2HFE (**Table 1**). **Fig. 9** shows the discharge capacity versus the discharge current density of Li-S coin-type cells. Among the [Li(dialkyl ether)$_3$][TFSA] electrolytes, the MPE-based HCE delivered the best rate performance with a discharge capacity of nearly 800 mAh g^{-1} at approximately 2.0 mA cm^{-2}. The excellent Li-ion transport properties can be considered as being predominantly responsible for the high rate capability of the cell with [Li(MPE)$_3$][TFSA]. However, the rate capability of Li-S batteries cannot be interpreted in terms of a single factor: the Li-ion transport properties. The rate capability of the cell using [Li(EPE)$_3$][TFSA] with a lower $\sigma \times t_{Li^+}^{abc}$ value was superior to that of the cell using [Li(BME)$_3$][TFSA]. One factor contributing to the lower rate capability of [Li(BME)$_3$][TFSA] is the aforementioned voltage dip. For example, the voltage dip reached 1.3 V for [Li(BME)$_3$][TFSA] but remained as high as 1.5 V for [Li(EPE)$_3$][TFSA] at the same discharge rate of 1/5 C, indicating that the nucleation overpotential of Li_2S is larger for [Li(BME)$_3$][TFSA]. Other electrode kinetics, such as the charge transfer resistance at the electrode interface, may also contribute to the rate capability. Further thorough investigations, including *operando* solubility measurements of the sulfur species, electrochemical studies of the charge transfer kinetics, and interfacial analysis of the S cathodes, would be required to fully understand the rate capability of Li-S batteries using sparingly solvating electrolytes.

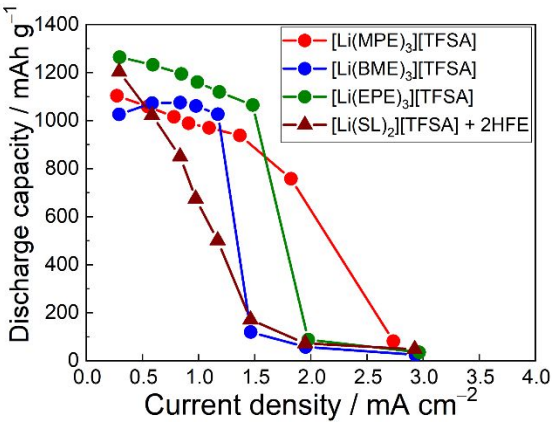

Fig. 9 Discharge capacity as a function of discharge current density for coin-type Li-S cells using sparingly solvating electrolytes at 30 ˚C.

Improvement of the gravimetric energy density is essential for the practical application of Li-S batteries. Lowering the overall weight of the battery, that is, reducing the amount of electrolyte in this study is a key approach for improving the energy density of the cells. To this end, we fabricated a Li-S battery using a pouch cell with a thicker S cathode (sulfur loading: 4.5 mg cm^{-2}) and smaller amount of electrolyte. The pouch cell configuration offers less excess space in the cell compared to coin-type cells, thereby allowing the amount of electrolyte to be significantly reduced. This enables the evaluation of high-energy-density Li-S cells under conditions similar to those of practical cells. Because of its high volatility of the solvent, [Li(MPE)$_3$][TFSA], which delivered higher rate performance, was found to be less suitable for pouch cell tests, which require a vacuum sealing process and precise control of the amount of electrolyte. Instead, we used [Li(BME)$_3$][TFSA] as the sparingly

solvating electrolyte and evaluated the cycle stability and gravimetric energy density with different electrolyte-to-sulfur (E/S) ratios in the range from 4 to 8 μL mg^{-1}.

Fig. 10a-c show the cycling dependence of the charge-discharge curves of pouch cells using $[Li(BME)_3][TFSA]$ at different E/S values. The initial discharge capacity exceeded 1100 mAh g^{-1} in all the pouch cells that were tested. The initial energy densities of these pouch cells are thus calculated as 314, 222, and 180 Wh kg^{-1} at E/S of 4, 6, and 8 μL mg^{-1}, respectively. Clearly, the amount of electrolyte has a significant impact on the energy density of the Li-S pouch cells. The pouch cells with $[Li(SL)_2][TFSA]$-2HFE delivered a slightly higher initial discharge capacity of 1311 mAh g^{-1} at the E/S ratio of 4 μL mg^{-1}; however, the initial energy density decreased to 261 Wh kg^{-1} due to the heavier nature of the electrolyte (**Fig. S3**). These results clearly demonstrate the benefits of the lightweight and sparingly solvating electrolytes based on dialkyl ethers, as discussed in the previous section.

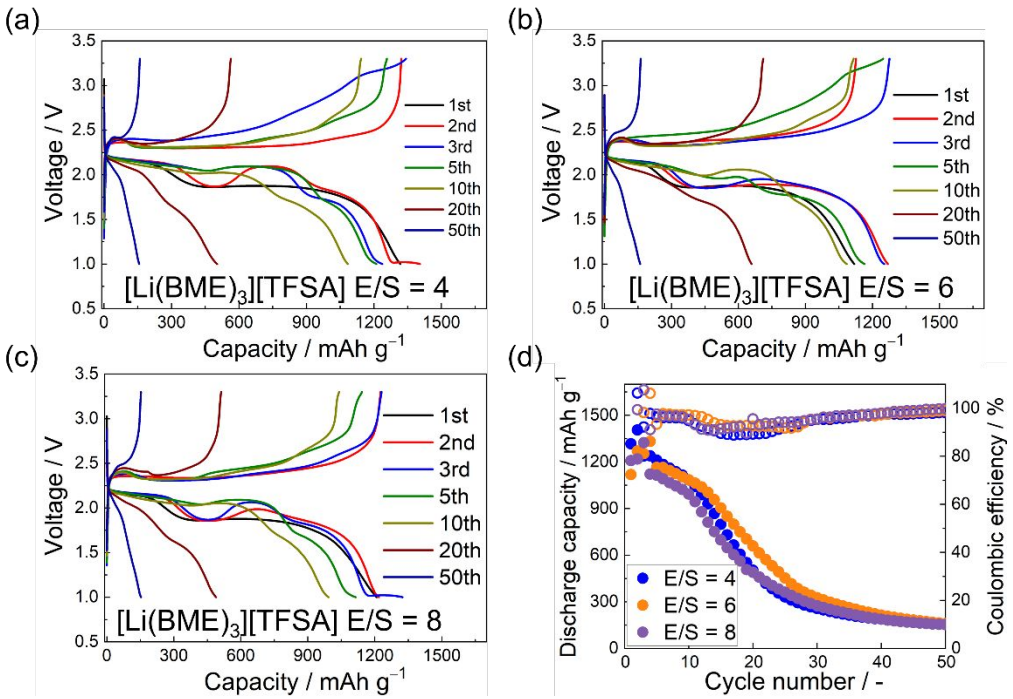

Fig. 10 Charge-discharge curves of Li-S pouch cells using [Li(BME)$_3$][TFSA] at E/S ratio of (a) 4 μL mg^{-1}, (b) 6 μL mg^{-1} and (c) 8 μL mg^{-1} at charge and discharge current densities of 1/20 C (1C = 7.3−8.1 mA cm^{-2}) with the cutoff voltage of 1.0 and 3.3 V at 30 ˚C. Sulfur loading: 4.4-4.8 mg cm^{-2}.

The average Coulombic efficiency during cycling tests was higher for larger E/S ratios and found to be 94.4%, 95.7%, and 95.9% for E/S of 4, 6, and 8 μL mg^{-1}, respectively. The lower Coulombic efficiency at a lower E/S is presumably related to more pronounced electrolyte decomposition at the S cathode and Li metal anode. Furthermore, dendritic Li deposition and the formation of electrochemically inaccessible “dead” Li may be more prominent at low E/S, where the Li ion current flux is more easily localized at the Li metal anode. As shown in **Fig. 10d**, the average Coulombic efficiency was uncorrelated with the cycling ability in that the cycling ability was independent from

the E/S ratio. As charge-discharge cycling progressed, the discharge capacity gradually declined to 200 mAh g^{-1} at the 50th cycle. Unlike the results for the coin-type cells (at E/S of 22−23 μL mg^{-1}), the second plateau in the discharge curves at E/S of 4, 6, and 8 μL mg^{-1} was unstable and undulated to reach the first plateau voltage in the middle of the capacity range, probably due to a heterogenous reduction reaction. Previous studies based on surface analysis and reaction modeling found that localized Li_2S deposition is more likely to be promoted at the cathode/electrolyte interface because of the restricted mass transfer of Li ions. This led to the formation of a distribution of unreacted S_8 and reduced Li_2S deposits in the direction perpendicular to the surface in thick S cathodes under lean electrolyte conditions.[39] Surface-localized Li_2S deposition and the resulting heterogeneity of sulfur reduction are obstacles to Li ion transport to the porous S cathode, which decrease the utilization of active sulfur materials in the cathode. This is also responsible for the unstable discharge curves observed in pouch cells with dialkyl ether-based HCE, which ultimately lead to capacity decay during charge-discharge cycling. The realization of high Coulombic efficiency and high capacity retention during long-term charge-discharge cycling in high energy density Li-S cells would require the rational design of porous S cathodes and surface engineering of Li metal anodes, in addition to the optimization of the sparingly solvating electrolytes.

Conclusions

The solubility of Li_2S_8 and S_8 was studied in a variety of electrolyte solutions ranging from organic electrolyte solutions to dense ionic fluids such as ionic liquids and HCEs. The results showed that the DN_{NMR} and Hildebrand solubility parameter δ could serve as a guide for designing sparingly solvating electrolytes. Dialkyl ether-based electrolytes have emerged as potential candidates for sparingly solvating electrolytes because of the low solubility of Li_2S_8 and S_8, high reduction stability against Li metal anodes, chemical stability against nucleophilic attack by polysulfides, low density, and relatively high Li-ion transport properties (particularly a high $t_{Li^+}^{abc}$). Raman spectroscopy and MD simulations revealed that ion aggregates dominated the Li-ion coordination structures in the HCEs based on dialkyl ethers. Compared to dialkyl ethers with longer alkyl chains at both ends, methyl-terminated linear ethers such as BME afforded a slightly higher coordination number for the ethers and a slightly lower coordination number for TFSA anions owing to the lower steric hindrance for Li ion coordination, thereby providing a lower degree of ionic association, higher ionic conductivity, and lower $t_{Li^+}^{abc}$. In contrast, the steric crowding of dialkyl ethers with longer alkyl chains (e.g., EPE) resulted in a more pronounced ion association in the HCE region. In Li-S batteries, dialkyl ether-based HCEs were found to achieve higher rate performance than previously reported SL-based sparingly solvating electrolytes owing to their superior Li-ion transport properties. The lightweight characteristic of the dialkyl ether-based electrolytes was demonstrated to be essential for increasing the energy density in Li-S pouch cells to higher than 300 Wh kg^{-1} even at a relatively high E/S ratio of 4 μL mg^{-1}, which would be beneficial for higher reversibility and long-term charge-discharge cycling. The experimental and

computational implications of this study provide insights into rational material design for optimizing sparingly solvating electrolytes for high-energy-density Li-S batteries for practical applications.

AUTHOR INFORMATION

Corresponding Author

Kazuhide Ueno: E-mail: ueno-kazuhide-rc@ynu.ac.jp

Conflicts of interest

There are no conflicts to declare.

Acknowledgements

This study was supported in part by Japan Society for the Promotion of Science (JSPS) KAKENHI grants (Nos. 20H02837, 22K19082, 23KK0102, 22KJ1402, 23KJ0992, 22H00340 and 23K17370) and JST ALCA-SPRING (Grant Number JPMJAL1301), Japan. This study was based on the results obtained from the JPNP20004 project subsidized by the New Energy and Industrial Technology Development Organization (NEDO). The computations in this study were performed using the facilities of the Research Centre for Computational Science,

Okazaki, Japan (Project: 23-IMS-C095) and the Supercomputer Center, Institute for Solid State Physics, The University of Tokyo.

References

1. A. Manthiram, Y. Fu, S.-H. Chung, C. Zu and Y.-S. Su, *Chem. Rev.*, 2014, **114**, 11751-11787.

2. Q. Pang, X. Liang, C. Y. Kwok and L. F. Nazar, *Nat. Energy*, 2016, **1**, 16132.

3. X. Ji, K. T. Lee and L. F. Nazar, *Nat. Mater.*, 2009, **8**, 500-506.

4. Y. V. Mikhaylik and J. R. Akridge, *J. Electrochem. Soc.*, 2004, **151**, A1969.

5. J. Gao, M. A. Lowe, Y. Kiya and H. D. Abruña, *J. Phys. Chem. C*, 2011, **115**, 25132-25137.

6. S. S. Zhang, *J. Power Sources*, 2013, **231**, 153-162.

7. S. S. Zhang, *Electrochim. Acta*, 2012, **70**, 344-348.

8. L. Cheng, L. A. Curtiss, K. R. Zavadil, A. A. Gewirth, Y. Shao and K. G. Gallagher, *ACS Energy Lett.*, 2016, **1**, 503-509.

9. J.-W. Park, K. Ueno, N. Tachikawa, K. Dokko and M. Watanabe, *J. Phys. Chem. C*, 2013, **117**, 20531-20541.

10. E. S. Shin, K. Kim, S. H. Oh and W. I. Cho, *Chem. Comm.*, 2013, **49**, 2004-2006.

11. L. Suo, Y.-S. Hu, H. Li, M. Armand and L. Chen, *Nat. Comm.*, 2013, **4**, 1481.

12. N. Tachikawa, K. Yamauchi, E. Takashima, J.-W. Park, K. Dokko and M. Watanabe, *Chem.*

Comm., 2011, **47**, 8157-8159.

13. X. Cao, H. Jia, W. Xu and J.-G. Zhang, *J. Electrochem. Soc.*, 2021, **168**, 010522.

14. X. Peng, Y. Lin, Y. Wang, Y. Li and T. Zhao, *Nano Energy*, 2022, **96**, 107102.

15. C. Chang, Y. Yao, R. Li, Z. Cong, L. Li, Z. H. Guo, W. Hu and X. Pu, *J. Mater. Chem. A*, 2022, **10**, 9001-9009.

16. X. Ren, S. Chen, H. Lee, D. Mei, M. H. Engelhard, S. D. Burton, W. Zhao, J. Zheng, Q. Li, M. S. Ding, M. Schroeder, J. Alvarado, K. Xu, Y. S. Meng, J. Liu, J.-G. Zhang and W. Xu, *Chem*, 2018, **4**, 1877-1892.

17. M. Shin, H.-L. Wu, B. Narayanan, K. A. See, R. S. Assary, L. Zhu, R. T. Haasch, S. Zhang, Z. Zhang, L. A. Curtiss and A. A. Gewirth, *ACS Appl. Mater. Interfaces*, 2017, **9**, 39357-39370.

18. M. Cuisinier, P. E. Cabelguen, B. D. Adams, A. Garsuch, M. Balasubramanian and L. F. Nazar, *Energy Environ. Sci.*, 2014, **7**, 2697-2705.

19. M. Yanagi, K. Ueno, A. Ando, S. Li, Y. Matsumae, J. Liu, K. Dokko and M. Watanabe, *J. Electrochem. Soc.*, 2020, **167**, 070531.

20. A. Nakanishi, K. Ueno, D. Watanabe, Y. Ugata, Y. Matsumae, J. Liu, M. L. Thomas, K. Dokko and M. Watanabe, *J. Phys. Chem. C*, 2019, **123**, 14229-14238.

21. H.-J. Peng, J.-Q. Huang, X.-B. Cheng and Q. Zhang, *Adv. Energy Mater.*, 2017, **7**, 1700260.

22. C. Weller, S. Thieme, P. Härtel, H. Althues and S. Kaskel, *J. Electrochem. Soc.*, 2017, **164**, A3766.

23. M. Hagen, P. Fanz and J. Tübke, *J. Power Sources*, 2014, **264**, 30-34.

24. Y. Liu, Y. Elias, J. Meng, D. Aurbach, R. Zou, D. Xia and Q. Pang, *Joule*, 2021, **5**, 2323-2364.

25. Y. Jeoun, M.-S. Kim, S.-H. Lee, J. Hyun Um, Y.-E. Sung and S.-H. Yu, *Chem. Eng. J.*, 2022, **450**, 138209.

26. M. Zhao, B.-Q. Li, H.-J. Peng, H. Yuan, J.-Y. Wei and J.-Q. Huang, *Angew. Chem. Int. Ed.*, 2020, **59**, 12636-12652.

27. K. Dokko, N. Tachikawa, K. Yamauchi, M. Tsuchiya, A. Yamazaki, E. Takashima, J.-W. Park, K. Ueno, S. Seki, N. Serizawa and M. Watanabe, *J. Electrochem. Soc.*, 2013, **160**, A1304.

28. M. Schmeisser, P. Illner, R. Puchta, A. Zahl and R. van Eldik, *Chem. Eur. J.*, 2012, **18**, 10969-10982.

29. M. J. Frisch, G. W. Trucks, H. B. Schlegel, G. E. Scuseria, M. A. Robb, J. R. Cheeseman, G. Scalmani, V. Barone, G. A. Petersson, H. Nakatsuji, X. Li, M. Caricato, A. V. Marenich, J. Bloino, B. G. Janesko, R. Gomperts, B. Mennucci, H. P. Hratchian, J. V. Ortiz, A. F. Izmaylov, J. L. Sonnenberg, Williams, F. Ding, F. Lipparini, F. Egidi, J. Goings, B. Peng, A. Petrone, T. Henderson, D. Ranasinghe, V. G. Zakrzewski, J. Gao, N. Rega, G. Zheng, W. Liang, M. Hada, M. Ehara, K. Toyota, R. Fukuda, J. Hasegawa, M. Ishida, T. Nakajima, Y. Honda, O. Kitao, H. Nakai, T. Vreven, K. Throssell, J. A. Montgomery Jr., J. E. Peralta, F. Ogliaro, M. J. Bearpark, J. J. Heyd, E. N. Brothers, K. N. Kudin, V. N. Staroverov, T. A. Keith, R. Kobayashi, J. Normand, K. Raghavachari, A. P. Rendell, J. C. Burant, S. S. Iyengar, J. Tomasi, M. Cossi,

J. M. Millam, M. Klene, C. Adamo, R. Cammi, J. W. Ochterski, R. L. Martin, K. Morokuma, O. Farkas, J. B. Foresman and D. J. Fox, *Journal*, 2016.

30. A. D. Becke, *J. Chem. Phys.*, 1993, **98**, 5648-5652.

31. W. Shinoda and M. Mikami, *J. Comput. Chem.*, 2003, **24**, 920-930.

32. O. N. Starovoytov, *J. Phys. Chem. B*, 2021, **125**, 11242-11255.

33. S. Tsuzuki, S. Ikeda, W. Shinoda, K. Shigenobu, K. Ueno, K. Dokko and M. Watanabe, *J. Phys. Chem. B*, 2023, **127**, 6333-6341.

34. P. G. Bruce, J. Evans and C. A. Vincent, *Solid State Ion.*, 1988, **28-30**, 918-922.

35. M. Watanabe, S. Nagano, K. Sanui and N. Ogata, *Solid State Ion.*, 1988, **28-30**, 911-917.

36. M. D. Galluzzo, J. A. Maslyn, D. B. Shah and N. P. Balsara, *J. Chem. Phys.*, 2019, **151**, 020901.

37. K. Shigenobu, M. Shibata, K. Dokko, M. Watanabe, K. Fujii and K. Ueno, *Phys. Chem. Chem. Phys.*, 2021, **23**, 2622-2629.

38. J. Liu, S. Li, M. Marium, B. Wang, K. Ueno, K. Dokko and M. Watanabe, *Sustain. Energy Fuels*, 2021, **5**, 1821-1831.

39. S. Li, S. Ishikawa, J. Liu, K. Ueno, K. Dokko, G. Inoue and M. Watanabe, *Batter. Supercaps.*, 2022, **5**, e202100409.

40. S. Zhang, K. Ueno, K. Dokko and M. Watanabe, *Adv. Energy Mater.*, 2015, **5**, 1500117.

41. R. Steudel and T. Chivers, *Chem. Soc. Rev.*, 2019, **48**, 3279-3319.

42. K. Ueno, J.-W. Park, A. Yamazaki, T. Mandai, N. Tachikawa, K. Dokko and M. Watanabe, *J.*

Phys. Chem. C, 2013, **117**, 20509-20516.

43. J.-W. Park, K. Yamauchi, E. Takashima, N. Tachikawa, K. Ueno, K. Dokko and M. Watanabe, *J. Phys. Chem. C*, 2013, **117**, 4431-4440.

44. J. H. Hildebrand and R. L. Scott, *The Solubility Of Nonelectrolytes: Monograph Series, American Chemical Society, No. 17*, Literary Licensing, LLC, 2012.

45. S. Venkatram, C. Kim, A. Chandrasekaran and R. Ramprasad, *J. Chem. Inf. Model.*, 2019, **59**, 4188-4194.

46. A. Marciniak, *Journal*, 2010, **11**, 1973-1990.

47. V. Antón, J. Muñoz-Embid, M. Artal and C. Lafuente, *Fluid Ph. Equilib*, 2016, **417**, 7-18.

48. C. J. Sheehan and A. L. Bisio, *Rubber Chem. Technol.*, 1966, **39**, 149-192.

49. A. F. M. Barton, *CRC Handbook of Solubility Parameters and Other Cohesion Parameters, Second Edition*, Taylor & Francis, 1991.

50. J. Speight, *Lange's Handbook of Chemistry, Seventeenth Edition*, McGraw-Hill Education, New York, N.Y, 17th edition edn., 2016.

51. S. C. Kim, S. T. Oyakhire, C. Athanitis, J. Wang, Z. Zhang, W. Zhang, D. T. Boyle, M. S. Kim, Z. Yu, X. Gao, T. Sogade, E. Wu, J. Qin, Z. Bao, S. F. Bent and Y. Cui, *Proc. Natl. Acad. Sci. U.S.A.*, 2023, **120**, e2214357120.

52. C. Zhang, K. Ueno, A. Yamazaki, K. Yoshida, H. Moon, T. Mandai, Y. Umebayashi, K. Dokko and M. Watanabe, *J. Phys. Chem. B*, 2014, **118**, 5144-5153.

53. D. Dong, F. Sälzer, B. Roling and D. Bedrov, *Phys. Chem. Chem. Phys.*, 2018, **20**, 29174-29183.

54. K. Shigenobu, T. Sudoh, M. Tabuchi, S. Tsuzuki, W. Shinoda, K. Dokko, M. Watanabe and K. Ueno, *J. Non-Cryst. Solids: X*, 2021, **11-12**, 100071.

55. T. Liu, H. Li, J. Yue, J. Feng, M. Mao, X. Zhu, Y.-s. Hu, H. Li, X. Huang, L. Chen and L. Suo, *Angew. Chem. Int. Ed.*, 2021, **60**, 17547-17555.

56. H. Cheng, S. Zhang, B. Zhang and Y. Lu, *Small*, 2023, **19**, 2206375.

57. Z. Han, S. Li, M. Sun, R. He, W. Zhong, C. Yu, S. Cheng and J. Xie, *J. Energy Chem.*, 2022, **68**, 752-761.

58. Y. Kameda, Y. Umebayashi, M. Takeuchi, M. A. Wahab, S. Fukuda, S.-i. Ishiguro, M. Sasaki, Y. Amo and T. Usuki, *J. Phys. Chem. B*, 2007, **111**, 6104-6109.

59. D. M. Seo, P. D. Boyle, O. Borodin and W. A. Henderson, *RSC Adv.*, 2012, **2**, 8014-8019.

60. D. Brouillette, D. E. Irish, N. J. Taylor, G. Perron, M. Odziemkowski and J. E. Desnoyers, *Phys. Chem. Chem. Phys.*, 2002, **4**, 6063-6071.

61. D. M. Seo, O. A. Borodin, S. D. Han, P. D. Boyle and W. A. Henderson, *J. Electrochem. Soc.*, 2012, **159**.

62. Y. Umebayashi, T. Mitsugi, S. Fukuda, T. Fujimori, K. Fujii, R. Kanzaki, M. Takeuchi and S.-I. Ishiguro, *J. Phys. Chem. B*, 2007, **111**, 13028-13032.

63. R. A. Spurr and H. Zeitlin, *J. Am. Chem. Soc.*, 1950, **72**, 4832-4832.

64. L. S. Gabrielyan, *J. Mol. Liq.*, 2017, **229**, 217-220.

65. J. N. Canongia Lopes, M. F. Costa Gomes and A. A. H. Pádua, *J. Phys. Chem. B*, 2006, **110**, 16816-16818.

66. Y. Wang and G. A. Voth, *J. Am. Chem. Soc.*, 2005, **127**, 12192-12193.

67. O. Borodin, L. Suo, M. Gobet, X. Ren, F. Wang, A. Faraone, J. Peng, M. Olguin, M. Schroeder, M. S. Ding, E. Gobrogge, A. von Wald Cresce, S. Munoz, J. A. Dura, S. Greenbaum, C. Wang and K. Xu, *ACS Nano*, 2017, **11**, 10462-10471.

68. Y. Yin, Y. Yang, D. Cheng, M. Mayer, J. Holoubek, W. Li, G. Raghavendran, A. Liu, B. Lu, D. M. Davies, Z. Chen, O. Borodin and Y. S. Meng, *Nat. Energy*, 2022, **7**, 548-559.

69. Z.-K. Tang, J. S. Tse and L.-M. Liu, *J. Phys. Chem. Lett.*, 2016, **7**, 4795-4801.

70. S. Kondou, Y. Sakashita, X. Yang, K. Hashimoto, K. Dokko, M. Watanabe and K. Ueno, *ACS Appl. Mater. Interfaces*, 2022, **14**, 18324-18334.

71. T. Hou, W. Xu, X. Pei, L. Jiang, O. M. Yaghi and K. A. Persson, *J. Am. Chem. Soc.*, 2022, **144**, 13446-13450.

72. S. Tsuzuki, T. Kaneko, K. Sodeyama, Y. Umebayashi, W. Shinoda, S. Seki, K. Ueno, K. Dokko and M. Watanabe, *Phys. Chem. Chem. Phys.*, 2021, **23**, 6832-6840.

73. F. Y. Fan, W. H. Woodford, Z. Li, N. Baram, K. C. Smith, A. Helal, G. H. McKinley, W. C. Carter and Y.-M. Chiang, *Nano Lett.*, 2014, **14**, 2210-2218.